Supplement of Atmos. Chem. Phys., 19, 11821–11841, 2019
https://doi.org/10.5194/acp-19-11821-2019-supplement

Supplement of

European NO_x emissions in WRF-Chem derived from OMI: impacts on summertime surface ozone

Auke J. Visser et al.

Correspondence to: Auke J. Visser (auke.visser@wur.nl)

1 WRF-Chem namelist

Table S1: Parameterization schemes used in the WRF-Chem setup.

WRF-Chem option	Parameterization scheme (reference)
Physics	
Microphysics	Morrison double-moment (Morrison et al. , 2009)
Longwave radiation	CAM (Collins et al. , 2004)
Shortwave radiation	CAM (Collins et al. , 2004)
Surface layer	MYNN2 (Nakanishi & Niino, 2006)
Land surface physics	Noah land surface model (Tewari et al. , 2004)
Boundary layer physics	MYNN2 (Nakanishi & Niino, 2006; Nakanasi & Niino, 2009)
Cumulus parameterization	Grell 3D Ensemble Scheme (Grell & Devenyi, 2002)
Lightning physics	PR92 neutral buoyancy (Price & Rind, 1993)
Chemistry	
Gas-phase chemistry	CBM-Z (Zaveri & Peters, 1999)
Photolysis parameterization	Madronich F-TUV (Tie et al. , 2003)

2 Meteorology evaluation

2.1 Meteorological reanalysis data

A European-wide meteorology evaluation performed by Mar et al. (2016) and numerous other studies demonstrated the skill of WRF-Chem to simulate several meteorological variables relevant to O_3 formation (radiation, temperature, wind speed and wind direction, boundary layer height). We further evaluated WRF-Chem's performance to simulate meteorology by comparing to the ERA-Interim reanalysis product (Dee et al. , 2011), for five variables that are important for surface ozone: surface pressure, 2m temperature, relative humidity, wind speed and wind direction. This complements the comparison with meteorological station observations (e.g. Mar et al. , 2016), and has the additional advantage that it is continuous in space.

2.2 Results

To evaluate the meteorology in WRF-Chem we perform a comparison with the state-of-the-art ECMWF operational reanalysis product (hereafter referred to as ECMWF reanalysis). Model performance metrics for the meteorological evaluation for the two simulated months are shown in Table S2, for which show the monthly average of single-day comparisons. We only calculate performance metrics for land-based pixels, as the oceanic pixels generally contribute less to the overall bias. Overall, WRF-Chem shows good performance compared to ECMWF-reanalysis data, and WRF-Chem-ECMWF differences between March and July are consistent in sign.

WRF-Chem performs best at simulating surface temperature and pressure, but relative humidity and wind speed and -direction are simulated with less accuracy. Surface temperature is slightly underestimated, which agrees well with the cold bias generally found in WRF(-Chem) (e.g. Holtslag et al. , 2013; Kleczek et al. , 2014). Surface pressure is in general slightly underestimated, although we must note that this comparison is limited by terrain height differences in ECMWF reanalysis compared to WRF-Chem. Relative humidity is overestimated substantially in WRF-Chem, by approximately 10%. This potentially impacts simulated surface ozone in WRF-Chem, as there is an important role for surface atmospheric humidity, which governs the VPD in combination with temperature, in describing ozone removal at the surface (Kavassalis & Murphy, 2017).

We found an approximately linear increase in the model bias (defined in this section as WRF-Chem - ECMWF reanalysis) for RH in July, with a slope of 0.2% d^{-1}. This coincides with a linear decrease in the bias from 0.12 K to -0.98 K, which would suggest that the domain-averaged latent energy flux is overestimated, leading to an enhanced moisture flux to the atmosphere and underestimated temperatures. For all other variables we did not observe a clear change in domain-average model biases with time, indicating that model performance is robust over the simulation period. Overall, this evaluation, in combination with recent WRF-Chem meteorology evaluation studies (e.g. Mar et al. , 2016) provides confidence in WRF-Chem's skill to reproduce domain-averaged surface meteorological conditions.

Table S2: Meteorological evaluation of two one-month WRF-Chem simulations with ECMWF operational reanalysis fields for five key surface meteorological variables. Only land-based pixels are used in the evaluation.

	March					July				
	μ_{ERA}	μ_{WRF}	r^2	MB	RMSE	μ_{ERA}	μ_{WRF}	r^2	MB	RMSE
T_{2m} [K]	281.51	280.52	0.77	-0.95	2.86	296.33	295.38	0.87	-0.95	2.69
P_{sfc} [hPa]	978.90	976.61	0.83	-2.29	18.56	972.94	972.28	0.96	-0.67	7.98
RH [%]	61.74	71.55	0.41	9.81	18.19	53.21	63.81	0.42	10.60	19.11
WS_{10m} [m s^{-1}]	4.78	5.45	0.56	0.68	2.08	3.34	4.51	0.50	1.17	1.95
WD_{10m} [°]	181.70	180.39	0.44	1.30	82.53	215.18	209.83	0.34	-5.35	85.71

3 Emission speciation

Table S3: Distribution of TNO-MACC non-methane VOC emission categories over VOC species in CBM-Z.

CBM-Z	TNO-MACC-III
e_ch3oh	alcohols
e_c2h5oh	alcohols
e_hc3	propane, butanes, ethyne
e_hc5	pentanes
e_hc8	hexanes & higher alkanes
e_ol2	ethene
e_olt	propene
e_oli	other alk(adi)enes & alkynes
e_tol	benzene, toluene, other aROUatics
e_xyl	xylene, trimethylbenzenes
e_hcho	methanal
e_ald	other alkanals, ethers
e_ket	ketones
e_ora2	acids

4 Spatial plots of emission scaling parameters

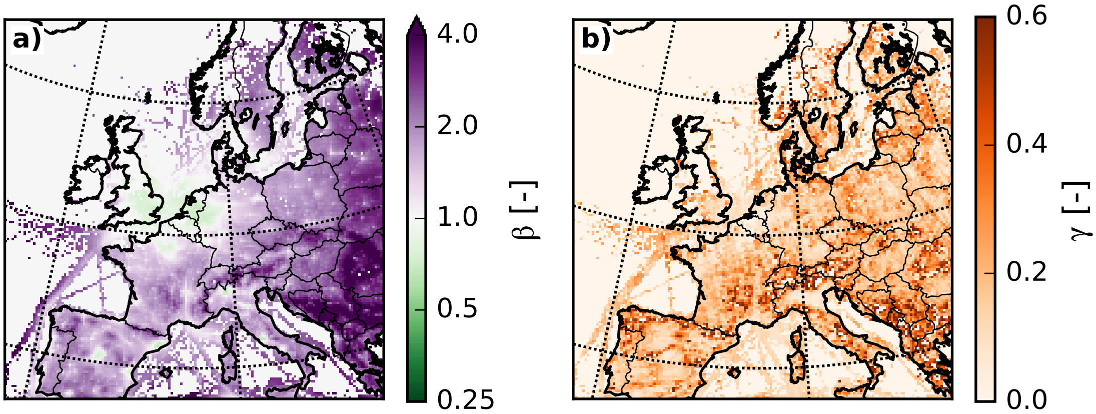

Figure S1: Spatial plots of monthly-averaged values of a) β and b) γ, calculated following Eqns. 3 and 4 (in main text), respectively.

5 Sensitivity study on inorganic reaction rates

A recent study investigated the representation of inorganic rate constants for tropospheric O_3 formation in WRF-Chem, and found a strong impact on the monthly average of 8 µg m^{-3} when using

MOZART inorganic rate constants in RADM2 (Mar et al. , 2016). To evaluate the potential impact of this on our simulations, we apply the mixed-layer and chemistry model MXLCH (Janssen et al. , 2012), which uses a simplified version of the MOZART mechanism. We set up this case as follows in order reproduce polluted conditions occurring in the Mediterranean, in order to determine the impact of inorganic reaction rates on the production of ozone in a well-mixed boundary layer: The location is set at 45.5°N/3.4°E (Southern France), initial O_3 concentrations in the mixed layer and the free troposphere are set to 62 ppbv and 78 ppbv, respectively, initial NO and NO_2 concentrations in the mixed layer are set to 1.6 ppb and 4.0 ppb, respectively, we apply NO and CO emission fluxes representative for relatively polluted conditions (0.15 ppb s^{-1} and 2.0 ppb s^{-1}, respectively), and we add two reactions to this mechanism representing HO_x cycling via reaction with O_3.

From a comparison of rate constants among the mechanisms CBM-Z, RADM2 and MOZART, we found the largest differences in rate constants for the reaction forming HNO_3 (NO_2 + OH + M $\longrightarrow HNO_3 + M$), while other inorganic rate constants are much more comparable. This is in line with the rate constant comparison by Knote et al. (2015). We modify the temperature-dependent rate constants of the reaction forming HNO_3 ($k_{NO_2\,+\,OH}$) according to Fig. S2 (panel a), and subsequently we study the sensitivity of afternoon ozone concentrations to $k_{NO_2\,+\,OH}$.

The NO_2 concentration and lifetime increase with decreasing rate constants, but the impact of $k_{NO_2\,+\,OH}$ on NO_2 concentrations is rather small (Fig. S2c). The relative impact on OH is stronger (Fig. S2d): the NO_2 availability in combination with $k_{NO_2\,+\,OH}$ drives OH loss, causing increasing OH concentrations for a decrease in k_{NO_2+OH}.

HNO_3 formation in CBM-Z has a somewhat lower rate constant compared to other mechanisms, and therefore leads to a longer NO_2 lifetime. This accelerates O_3 formation, and thus leads to higher afternoon O_3 concentrations. The upper right panel of Fig. S2 shows that the inter-mechanism spread is ±2 ppbv. From this sensitivity analysis with a simplified representation of atmospheric chemistry within the atmospheric boundary layer, we conclude that there is some sensitivity of afternoon O_3 concentrations to the representation of inorganic reactions, particularly HNO_3 formation, involved in O_3 chemistry.

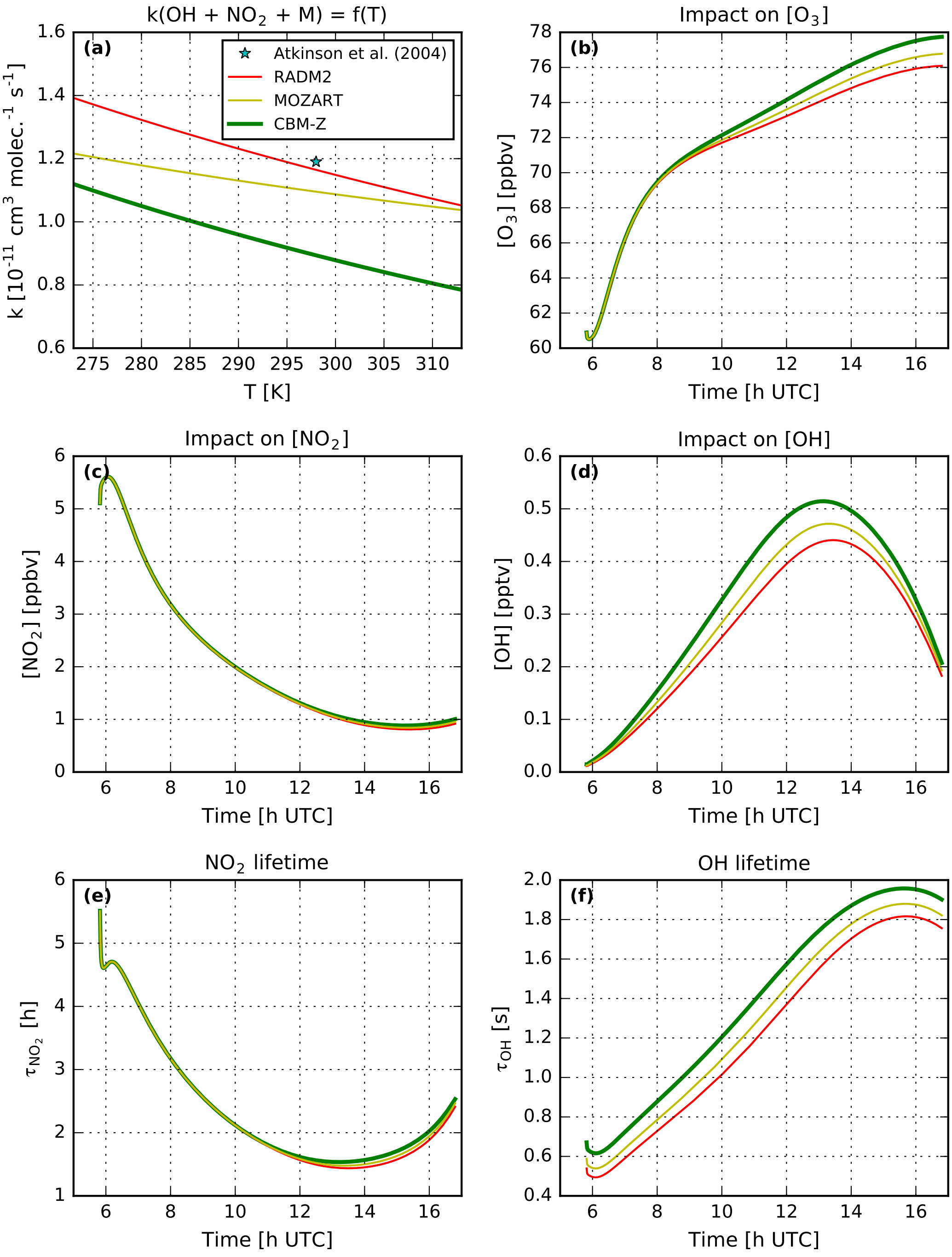

Figure S2: Temperature-dependence of rate constants for the reaction $NO_2 + OH + M \longrightarrow HNO_3 + M$ from three different mechanisms (panel a), and the resulting impacts on O_3 (pabel b), NO_2 (c) and OH (d). Panel a additionally gives the IUPAC-recommended value under standard conditions (P = 1 bar, T = 298 K) given by Atkinson et al. (2004). The lifetimes of NO_2 and OH are given in panels e and f, respectively.

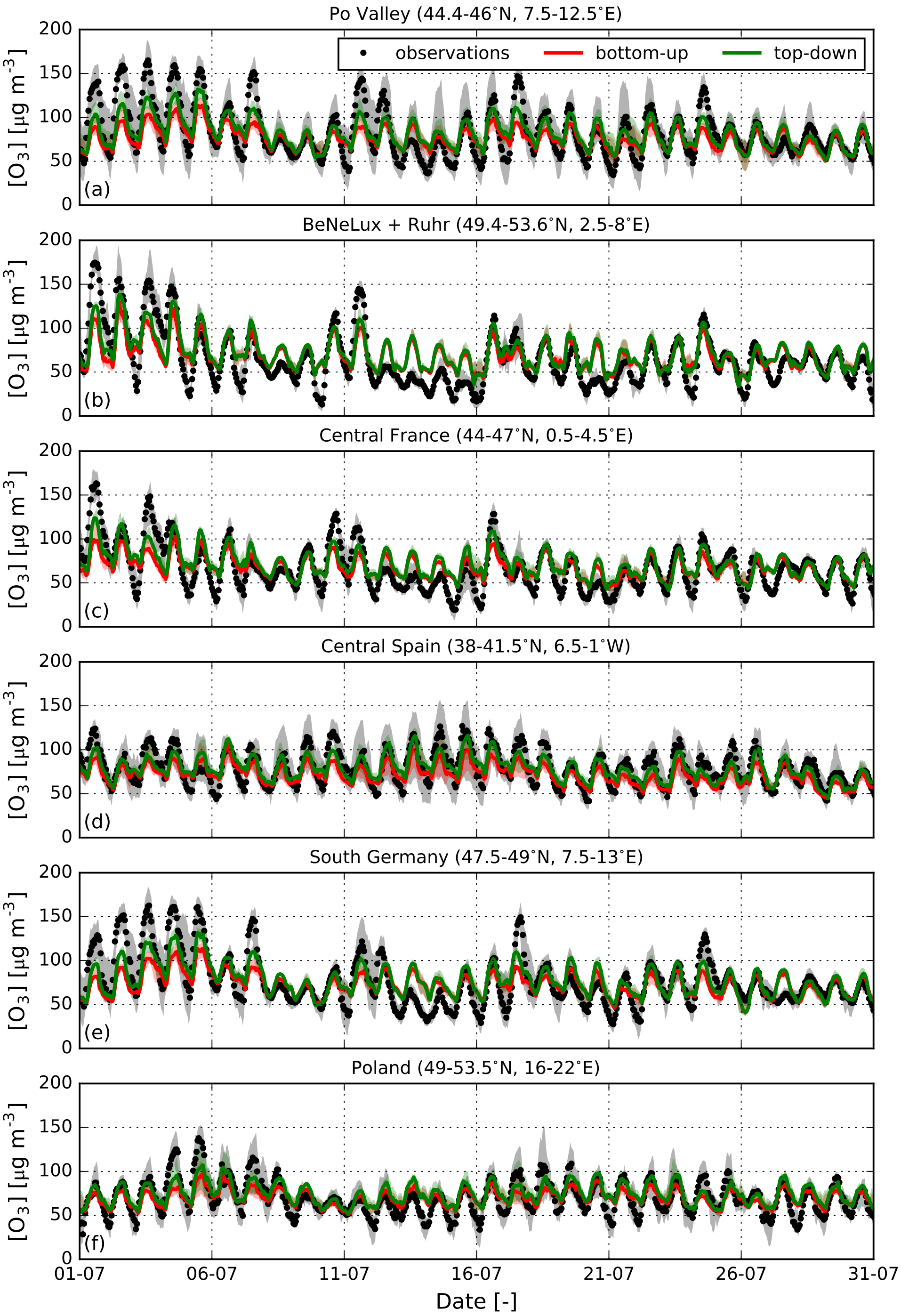

Figure S3: July 2015 time series of the median (shaded areas show inter-quartile range) O_3 concentrations as observed at AirBase stations (black dots), and as simulated by WRF-chem with bottom-up (red) and top-down emissions (green). Medians are calculated by including all stations (resp. co-sampled simulations) in the latitude/longitude range specified in the subplot titles.

Table S4: Model performance statistics for surface ozone concentration time series of the WRF-Chem simulation with bottom-up and top-down emissions for six European regions.

	Po Valley	BeNeLux + Ruhr	Central France	Central Spain	South Germany	Poland
n (stations)	59	32	29	24	39	18
	Bottom-up					
MBE	-20.14	16.82	3.35	-22.40	-11.15	1.74
RMSE	68.07	71.48	59.92	45.39	68.68	43.64
r	0.80	0.78	0.76	0.81	0.74	0.77
	Top-down					
MBE	-1.58	25.94	17.29	-1.33	5.02	16.10
RMSE	55.08	68.57	56.48	36.44	58.13	41.81
r	0.85	0.81	0.79	0.83	0.81	0.80

References

Atkinson, R, Baulch, D L, Cox, R A, Crowley, J N, Hampson, R F, Hynes, R G, Jenkin, M E, Rossi, M J, & Troe, J. 2004. Evaluated kinetic and photochemical data for atmospheric chemistry: Volume I - gas phase reactions of Ox, HOx, NOx and SOx species. Atmospheric Chemistry and Physics, **4**(6), 1461–1738.

Collins, W. D., Rasch, P. J., Boville, B.A., Hack, J. J., McCaa, J. R., Williamson, D. L., Kiehl, J. T., Briegleb, B., Bitz, C., Lin, S., Zhang, M., & Dai, Y. 2004. Description of the NCAR community atmosphere model (CAM 3.0). Tech. rept. National Center for Atmospheric Research, Boulder, CO.

Dee, D. P., Uppala, S. M., Simmons, A. J., Berrisford, P., Poli, P., Kobayashi, S., Andrae, U., Balmaseda, M. A., Balsamo, G., Bauer, P., Bechtold, P., Beljaars, A. C M, van de Berg, L., Bidlot, J., Bormann, N., Delsol, C., Dragani, R., Fuentes, M., Geer, A. J., Haimberger, L., Healy, S. B., Hersbach, H., Hólm, E. V., Isaksen, L., Kållberg, P., Köhler, M., Matricardi, M., Mcnally, A. P., Monge-Sanz, B. M., Morcrette, J. J., Park, B. K., Peubey, C., de Rosnay, P., Tavolato, C., Thépaut, J. N., & Vitart, F. 2011. The ERA-Interim reanalysis: Configuration and performance of the data assimilation system. Quarterly Journal of the Royal Meteorological Society, **137**(656), 553–597.

Grell, G. A., & Devenyi, D. 2002. A generalized approach to parameterizing convection combining ensemble and data assimilation techniques. Geophysical Research Letters, **29**(14), 10–13.

Holtslag, A. A.M., Svensson, G., Baas, P., Basu, S., Beare, B., Beljaars, A. C.M., Bosveld, F. C., Cuxart, J., Lindvall, J., Steeneveld, G. J., Tjernström, M., & Van De Wiel, B. J.H. 2013. Stable atmospheric boundary layers and diurnal cycles: Challenges for weather and climate models. Bulletin of the American Meteorological Society, **94**(11), 1691–1706.

Janssen, R. H.H., Vilà-Guerau De Arellano, J., Ganzeveld, L. N., Kabat, P., Jimenez, J. L., Farmer, D. K., Van Heerwaarden, C. C., & Mammarella, I. 2012. Combined effects of surface conditions, boundary layer dynamics and chemistry on diurnal SOA evolution. Atmospheric Chemistry and Physics, **12**(15), 6827–6843.

Kavassalis, Sarah C., & Murphy, Jennifer G. 2017. Understanding ozone-meteorology correlations: A role for dry deposition. Geophysical Research Letters, **44**(6), 2922–2931.

Kleczek, Michal A., Steeneveld, Gert Jan, & Holtslag, Albert A.M. 2014. Evaluation of the Weather Research and Forecasting Mesoscale Model for GABLS3: Impact of Boundary-Layer Schemes, Boundary Conditions and Spin-Up. Boundary-Layer Meteorology, **152**(2), 213–243.

Knote, C., Tuccella, P., Curci, G., Emmons, L., Orlando, J. J., Madronich, S., Baró, R., Jiménez-Guerrero, P., Luecken, D., Hogrefe, C., Forkel, R., Werhahn, J., Hirtl, M., Pérez, J. L., San José, R., Giordano, L., Brunner, D., Yahya, K., & Zhang, Y. 2015. Influence of the choice of gas-phase mechanism on predictions of key gaseous pollutants during the AQMEII phase-2 intercomparison. Atmospheric Environment, **115**, 553–568.

Mar, Kathleen A, Ojha, Narendra, Pozzer, Andrea, & Butler, Tim M. 2016. Ozone air quality simulations with WRF-Chem (v3 . 5 . 1) over Europe : model evaluation and chemical mechanism comparison. Geoscientific Model Development, **9**, 3699–3728.

Morrison, H., Thompson, G., & Tatarskii, V. 2009. Impact of Cloud Microphysics on the Development of Trailing Stratiform Precipitation in a Simulated Squall Line: Comparison of One- and Two-Moment Schemes. Monthly Weather Review, **137**(3), 991–1007.

Nakanasi, M., & Niino, H. 2009. Development of an improved turbulence closure model for the atmospheric boundary layer. Journal of the Meteorological Society of Japan, **87**(5), 895–912.

Nakanishi, Mikio, & Niino, Hiroshi. 2006. An improved Mellor-Yamada Level-3 model: Its numerical stability and application to a regional prediction of advection fog. Boundary-Layer Meteorology, **119**(2), 397–407.

Price, C., & Rind, D. 1993. What determines the cloud-to-ground lightning fraction in thunderstorms? Geophysical Research Letters, **20**(6), 463–466.

Tewari, M, Chen, F, Wang, W, Dudhia, J, Lemone, M A, Mitchell, K, Ek, M, Gayno, G, Wegiel, J, & Cuenca, R H. 2004. Implementation and verification of the Unified Noah Land Surface model in the WRF model. Pages 11–15 of: 20th conference on weather analysis and forecasting/16th conference on numerical weather prediction.

Tie, Xuexi, Madronich, S., Walters, S., Zhang, R., Rasch, P. J., & Collins, William J. 2003. Effect of clouds on photolysis and oxidants in the troposphere. Journal of Geophysical Research, **108**(D20).

Zaveri, R.A., & Peters, L.K. 1999. A new lumped structure photochemical mechanism for large-scale applications. Journal of Geophysical Research: Atmospheres, **104**(D23), 30387–30415.